*Abd El-Aziz S. Fouda *[1], Aya M.Salem[2],*
Ahmed M. Wahba[3], Samir A. Abd El-Maksous[4],
Mahmoud N. EL-Haddad[1]

[1]*Mansoura University, Department of Chemistry, Faculty of Science, Mansoura- 35516, Egypt,* [2]*Department of Basic Science, Higher Institute of Electronic Engineering (HIEE), Belbis, Egypt,* [3]*Department of Basic Science, Higher Institute of Engineering and Technology (HIET), El-Mahalla, Egypt,* [4]*Port Said University, Department of Chemistry, Faculty of Science, Port Said, Egypt*

Experimental and theoretical optimization of *Chelidonium Majus (Papaveraceae)* extract as an environmentally friendly inhibitor for corrosion of α-brass in nitric acid solution

ABSTRACT

The research paper discusses the study of the inhibition rates of Chelidonium Majus (Papaveraceae) plant extract (CME) on α- brass in 1.0 M HNO₃ solution. The study was carried out using chemical and electrochemical techniques, which showed results of up to 97% inhibition with 150 ppm at 25⁰C. For the polarization results, CME is a mixed-type inhibitor. The increase in the charge transfer resistance and the decrease in the capacitance of the double layer with increasing concentration were observed by Nyquist diagrams and it was found that the inhibition process follows the Langmuir isotherm which proves the formation of a monolayer on the surface of the α- brass. Quantum chemical calculations were performed using the DFT method to determine the active centres of the CME which responsible for adsorption, as well, to their possible interaction mechanism with the- brass surface.

Keywords: *Corrosion inhibition, α- brass, HNO₃, Chelidonium Majus extract, DFT.*

1. INTRODUCTION

The phenomenon of metal corrosion has become a great danger that threatens many industries as well as the environment in general [1]. Therefore, efforts must be made to reduce the risks of corrosion in different industries. The use of inhibitors had a great practical effect in protecting metals from dissolution as a result of corrosion and this is done by adding simple percentages of inhibitors to the corrosive media [2]. Thus, it reduces and in some cases prevents the contact of aggressive ions on the surface of the metal or performs both processes [3]. Inorganic substances such as phosphates, chromates, dichromate, and arsenic are among most of the compounds used in industrial applications to inhibit the corrosion of many metals and alloys [4]. The high toxicity of these compounds has led to a limitation in their inhibitors and the search for more environmentally friendly alternatives that contain functional groups containing atoms of oxygen, nitrogen, or sulphur which have been approved as decay inhibitors [5].

The interest in green alternatives has increased in the last decade as a result of increased environmental awareness and the adoption of many strict regulations to preserve the environment. Natural alternatives have been used as antimicrobial [6], antifungal [7], anticancer [8], and antibacterial activities [9]. Several efforts are being made to develop compounds suitable for use as corrosion inhibitors in different media. This research is based on the use of environmentally friendly plant extracts to inhibit the corrosion of metals and alloys. The use of plant extracts as corrosion inhibitors, as the following research indicates this role. Calicotome extract [10], Hibiscus rosa-sinensis Linn [11], Beet root extract in well water [12], spirulina solution which confirms with electrochemical techniques [13], spirulina [14]. The present work aims to find a naturally occurring cheap and environmentally safe substance that could be used for inhibiting the corrosion of α-brass. The use of the natural product will establish, simultaneously, the economic and environmental goals". In several research, plant extracts have been mentioned as prospective agents to lessen corrosion in different industrial solutions [15,16]. As reported previously, the ethanolic extract of (CME) contains major levels of isoquinoline alkaloids compounds such as 6,7,12b,13-Tetrahydro- H-

---
*Corresponding author: *Abd El-Aziz S. Fouda*

E-mail: asfouda@hotmail.com

"bis[1,3] benzodioxolo [5,6-a:4',5'-g] quinolizine (stylopine)",(5bR,6S,12bS)-13-Methyl-5b,6,7,12b, 13,14-hexahydro-2H,10H-[1,3]benzodioxolo[5,6-c] [1,3]dioxolo[4,5-i] phenanthridin-6-ol (chelidonine), (Z)-7-methyl-6,16-dihydro-[1,3] dioxolo[4',5':5,6] benzo[1,2-c] [1,3] dioxolo [5', 4': 4, 5]"Benzo [1,2-g]azecin-15(7H)-one (protopine), and 3,4-Dimethoxy-6-methyl-5,7,8,15-tetrahydro-11H-[1,3] benzodioxolo [5,6-e][2] benzazecin-14(6H)-one (allocryptopine). In some literature, oxygen, nitrogen atoms, and aromatic rings are considered the centers of adsorption in the four ingredients [17]. As a result, (CME) may be studied as safe corrosion inhibitor. Our work examined the inhibitory effect of this extract on α -brass in 1.0M HNO_3 acid using weight loss (WL), potentiodynamic polarization (PP), and electrochemical impedance spectroscopy (EIS). A Scanning Electron Microscope (SEM) was used to determine whether the shape of the α-brass surface changed after immersion in 1.0M HNO_3 solution with or without the inhibitor (SEM). By using quantum chemical calculations at the DFT level, the correlation of experimental data and major functional components of (CME) were discussed.

2. EXPERIMENTAL SECTION

2.1. Preparation of (CME) Extract

To prepare the plant extract, dried leaves of the Chelidonium Majus plant were used and soaked in an ethanol solution. After 48 hours, using filter papers, the unwanted objects were removed and then heated to get rid of the ethanol. Deionized water was used to prepare the different concentrations used in the research. The molecular structures of stylopine, chelidonine, protopine, and allocryptopine are revealed in Fig. 1.
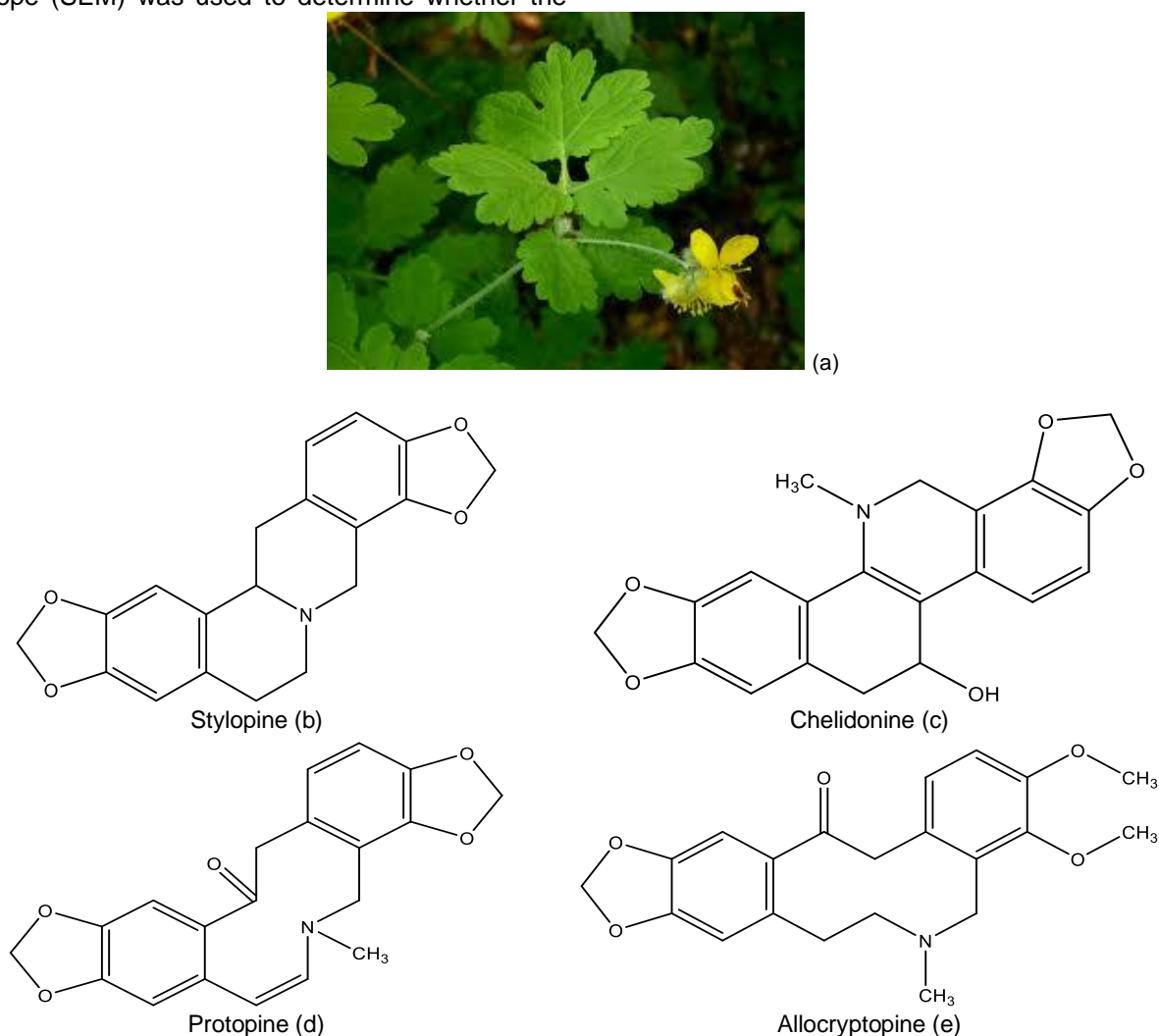

(a)

Stylopine (b)

Chelidonine (c)

Protopine (d)

Allocryptopine (e)

Figure 1. Image of CM leaves (a), and their chemical structure constituents: Stylopine (b), Chelidonine (c), Protopine (d), and Allocryptopine (e)

Slika 1. Slika CM listova (a) i njihovih sastojaka hemijske strukture: stilopin (b), helidonin (c) protopin (d) i alokriptopin (e)

2.2. Materials preparation

For weight loss studies, α-brass was used with a composition of (70% Cu and 30% Zn), where the coupons were formed with different dimensions of (2 × 2 × 0.1 cm) and dimensions (1 × 1 × 0.1 cm) for the electrochemical measurement's studies. The samples were polished with sandpaper of different grades, and then washed with deionized water and then alcohol to remove dirt and greases, and deionized water was used in all preparations. A solution of 1.0M HNO_3 was used as a corrosive medium for all measurements and was prepared from analytical-grade nitric acid. The CME was diluted in 1.0M HNO_3 corrosion medium to prepare (25, 50, 75,100, 125, and 150 ppm) test solution, respectively [18, 19].

2.3. WL measurements

For WL measurements, a sheet of α-brass with a size of (2 × 2 × 0.1 cm) was used, polished by different degrees of sandpaper, and then washed with double distilled water, followed by alcohol to get rid of dirt, and good drying and weighing. The weight is followed by the use of traditional methods for measuring WL at temperatures of ($25 - 45^0$C). With the extracted results, the values of (% IE_{WL}) of the inhibitor, the degree of surface coverage (θ), and corrosion rates (CR) were determined using the following equations [20]:

$$\%IE_{WL} = \left(\frac{W_1 - W_2}{W_1}\right) x\ 100 = \theta\ x\ 10 \qquad (1)$$

$$CR = \frac{W}{t} \qquad\qquad (2)$$

where W_1 is the WL for α-brass with the extract, W_2 WL for α-brass without the extract, t is the time of immersion (min), and (W) is the WL of α-brass after the time (t).

2.4. Electrochemical measurements

A conventional three-electrode cell was used to complete the electrochemical measurements. The cell consisted of a working electrode as α- brass, a platinum sheet (1.0 cm^2) as a reference electrode, and saturated calomel (SCE) as the counter electrode [21]. The PP and EIS measurements were used to study the electrochemical behavior of the corrosion of α- brass in 1.0M HNO_3 medium. The Gamry Instrument Series G 750™ - Potentiostat/ Galvanostat/ ZRA device) was used for these electrochemical measurements, A voltage survey was carried out at a rate of 1.0 mV/s from the potential value of corrosion in the negative direction, which started from (-600 mV to +600 mV) open circuit potential (E_{ocp}) using newly prepared solutions at 25^0C. At the OCP, EIS tests were performed at frequencies between 10^{+6}Hz and 10^{+1} Hz with amplitude of ±10 mV. All results were obtained and the process was carried out 3 times to ensure the validity of the results.

2.5. Theoretical calculations

Gaussian 09 software (Gaussian, Inc., CT, USA) was used to perform quantum chemical calculations using generalized density functional theory (DFT) with the Becke three parameters Lee, Yang, and Parr (B3LYP). Based on 6-311G++ (d,p), the electronic properties of many organic compounds and their geometries can be accurately determined. Calculations were carried out in the gas phase for all quantum chemical calculations [22].

3. RESULTS AND DISCUSSION

3.1. WL method

This method was used to calculate the inhibition ratios at temperatures of (25-45°C) according to equation (1). Depending on the results, CR and % IE_{WL} values were calculated for the CME. The results are shown in Fig. 2, and Table 1.

Table 1. Effect of CME concentrations on CR and (% IE_{WL}) for α-brass in 1.0 M HNO_3

Tabela 1. Uticaj koncentracija CME na CR i (% IEVL) za α -mesing u 1.0 M HNO_3

Temp	25 ºC		30 ºC		35 ºC		40 ºC		45 ºC	
Conc. ppm	CR, mgcm^{-2} min^{-1}	% IEWL	CR, mgcm^{-2} min^{-1}	% IEWL	CR, mg cm^{-2} min^{-1}	% IEWL	CR, mg cm^{-2} min^{-1}	% IEWL	CR, mg cm^{-2} min^{-1}	% IEWL
Blank	1.945	-----	2.011	----	2.121	-----	2.197	-----	2.218	-----
25	0.289	85.1	0.380	81.1	0.483	77.2	0.573	73.9	0.672	69.7
50	0.190	90.2	0.285	85.8	0.343	83.8	0.421	80.8	0.512	76.9
75	0.144	92.5	0.229	88.6	0.309	85.4	0.397	81.9	0.492	77.8
100	0.107	94.5	0.193	90.4	0.241	88.6	0.331	84.9	0.428	80.7
125	0.087	95.5	0.146	92.7	0.207	90.2	0.282	87.2	0.269	83.8
150	0.056	97.1	0.130	93.5	0.180	91.5	0.217	90.1	0.211	86.4

The results proved that adding an amount greater than CME increases the inhibition ratios, which were found to decrease with increasing temperature, and this is due to the occurrence of desorption of the plant extract on the surface of the metal [23]. It was found that the highest inhibition rate reached 97%, which was obtained at 150 ppm, and it was approved as the best concentration for the inhibition process. With these results, we conclude the high efficiency of this plant extract in the process of inhibiting corrosion α-brass in 1.0 M HNO₃ solution.
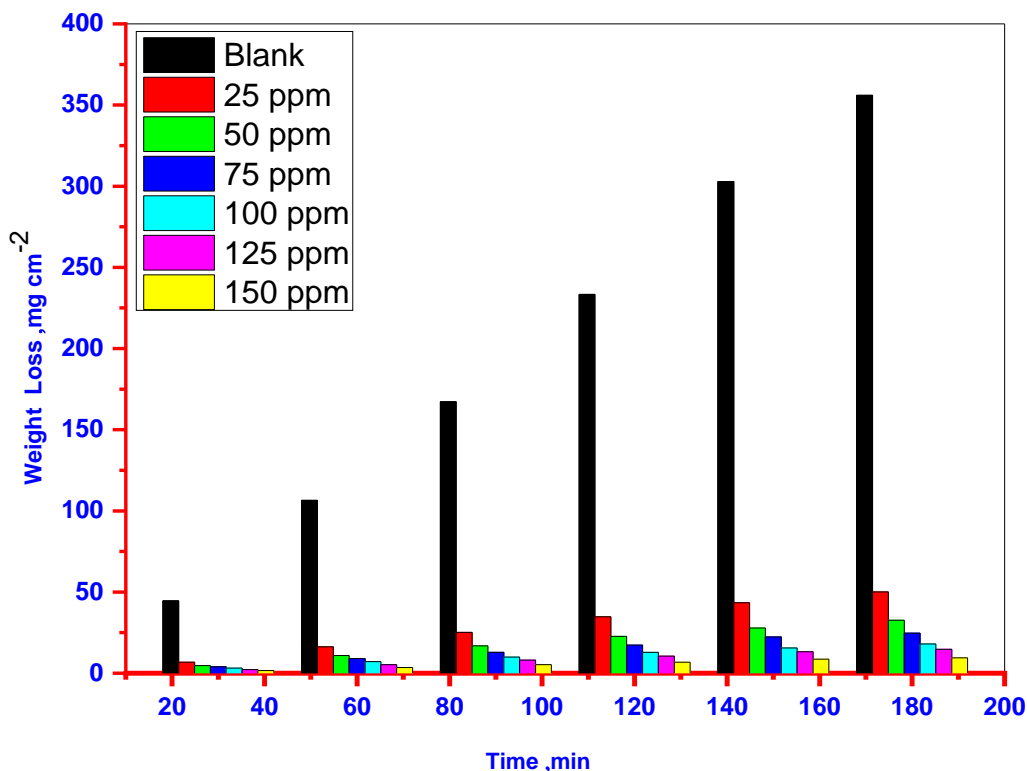

Figure 2. WL-time curves for α-brass in 1.0 M HNO₃ solution with/ without CME at 25ºC

Slika 2. WL-vremenske krive za α -mesing u 1.0 M rastvoru HNO₃ sa/ bez CME na 25⁰C

3.2 Effect of temperature

The simplicity and availability of the WL technique led to its use on a large scale, as it was used to study the effect of temperature on the rate of corrosion of α-brass with the addition of varying amounts of CME extract in a solution of 1.0M HNO₃ solution for a period of up to 180 minutes at temperatures ranging from 25 - 45ºC and which are recorded in Table 1. This Table demonstrates that the rate at which alpha brass corrodes increase as the temperature rises and at the same time the percentages of the %IE$_{WL}$ of CME decrease by the increasing the temperature. This confirms that the process of adsorption of the plant extract on the surface of α-brass is carried out through physical adsorption with weak bonds [24].

The values of ΔS*and ΔH* for blank and also for several concentrations of CME were studied for α-brass in 1.0M HNO₃ solution using Arrhenius plot as log CR against 1/T, and log CR/T vs 1/T (Figs.3

& 4), respectively), according to the following equations [27]:

$$CR = Ae^{\left(-\frac{E_a^*}{RT}\right)} \qquad (3)$$

$$CR = \frac{RT}{Nh}e^{\left(\frac{\Delta S^*}{R}-\frac{\Delta H^*}{RT}\right)} \qquad (4)$$

as E^*_a is the activation energy, R is the universal gas constant, T is the absolute temperature, A is the frequency factor, h is Planck's constant, and N is Avogadro's number. Where straight lines are obtained with a slope of (ΔH*/R) and an intersection of (log R/Nh + ΔS*/R). It was observed that by increasing the concentration of the CME, the activation energy values increased, this indicates the rise in the surface adsorbent layer development., and thus the energy required to break the barrier during corrosion increases [25, 26].
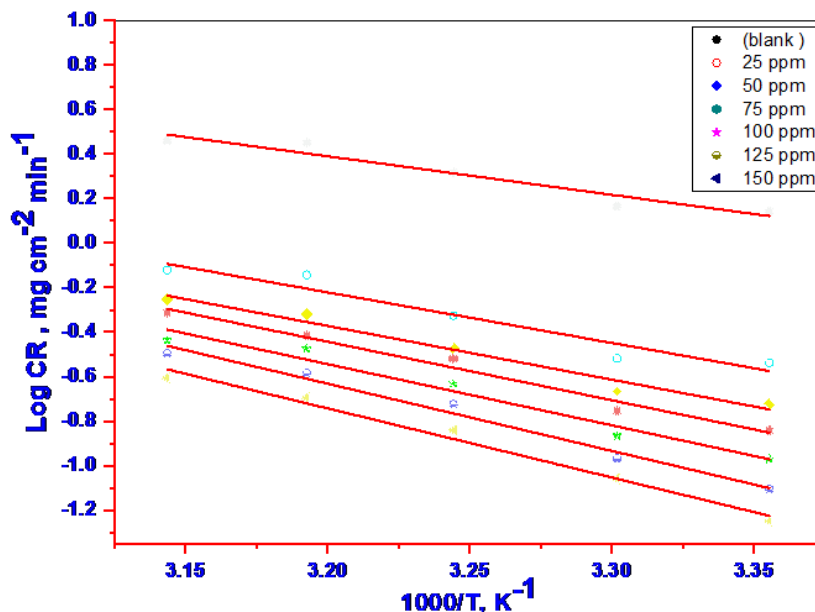
Figure 3. Log CR versus 1/T for α-brass in 1.0 M HNO₃ with and without CME

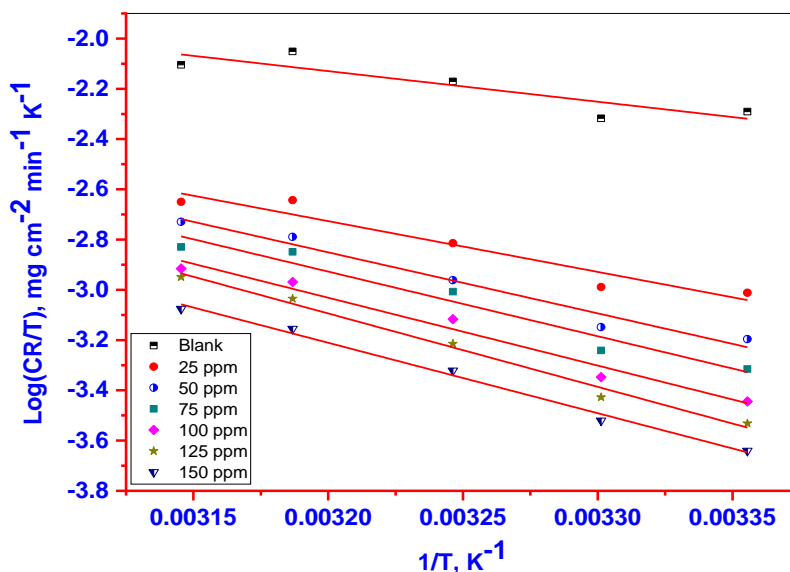*Slika 3. Log CR naspram 1/T za α -mesing u 1.0M HNO₃ sa i bez CME*

Figure 4. Log (CR/T) versus 1/T for α- brass in 1.0 M HNO₃ as blank and with CME

Slika 4. Log (CR/T) u odnosu na 1/T za α- mesing u 1.0 M HNO₃ kao prazno i sa CME

Table 2. Kinetic activation parameters for α-brass corrosion in 1.0 M HNO₃ without/ with of CME

Tabela 2. Kinetički aktivacioni parametri za koroziju α-mesinga u 1.0 M HNO₃ bez/sa CME

Conc., ppm	Ea*, kJ mol-1	-Δ H*, kJ mol-1	-ΔS*, J mol-1K-1
Blank	**10.7±0.145712**	**13.2±0.153096**	**148.6±0.22443**
25	37.5±0.230940	40.0±0.173205	74.3±0.115470
50	42.7±0.088191	45.2±0.152752	60.1±0.260341
75	52.6±0.208166	55.2±0.202758	29.8±0.088191
100	56.3±0.145296	58.9±0.145296	18.7±0.145296
125	59.9±0.173205	62.4±0.088191	8.7±0.1201850
150	66.1±0.115470	68.7±0.066666	9.6±0.1763834

3.3. Adsorption Isotherms

The thermal isotherms consider that the corrosion process depends mainly on the surface coverage (θ) and therefore it is another aspect of IE, i.e. θ = IE/100. Many efforts have been made to adopt a relationship between the degree of coverage (θ) and the highest concentration of the inhibitor at a certain temperature and it was found that the Langmuir adsorption isotherm is the best curve to describe the inhibitory performance For the plant extract (Fig. 5), which assumes that the metal surface has a fixed number of adsorption centers and that each center has one adsorbent type, which can be indicated by the following equation [27]:

$$\frac{C}{\theta} = \frac{1}{K_{ads}} + C \tag{5}$$

As *C*, the inhibitor concentration (mol./L), and K_{ads} are related to (ΔG°_{ads}) acceding to the relation:

$$K_{ads} = \frac{1}{55.5} \, e^{\left(\frac{-\Delta G^{\circ}_{ads}}{RT}\right)} \tag{6}$$

As 55.5 in mol./ L is the concentration of H_2O on the metal surface. Table 3 shows the values of ΔG°_{ads} as a function of temperature at average temperatures ranging from 298 - 318 K. From the results, we conclude that ΔG°_{ads} is highly dependent on temperature by drawing the relationship between ΔG°_{ads} and T (Fig. 6). The entropy (ΔS°_{ads}) and enthalpy of adsorption (ΔH°_{ads}) can be calculated according to the equation [28]:

$$\Delta G^{\circ}_{ads} = \Delta H^{\circ}_{ads} - T\Delta S^{\circ}_{ads} \tag{7}$$

The spontaneous adsorption of the extract on the α-brass surface can be indicated by the negative ΔG°_{ads} values increased with the increase of %IE values, which confirms the stability of the adsorbent layer physical adsorption [29]. We find that with an increase of ΔG°_{ads}, the values of the inhibition ratios increase and we conclude that the adsorption of the extract on the α-brass surface is an exothermic process through the negative sign of ΔH°_{ads}, which means that %IE decreases with the increase in temperature [30]. On the other hand, the positive value of ΔS^{o}_{ads} is attributed to the increase of solvent entropy as disorder occurs at the metal/solution interface. This is attributed to the displacement of H_2O molecules by CME molecules on the metal surface in the test medium.

Table 3. Thermodynamic parameters of CME were obtained from adsorption isotherm

Tabela 3. Termodinamički parametri CME dobijeni iz izoterme adsorpcije

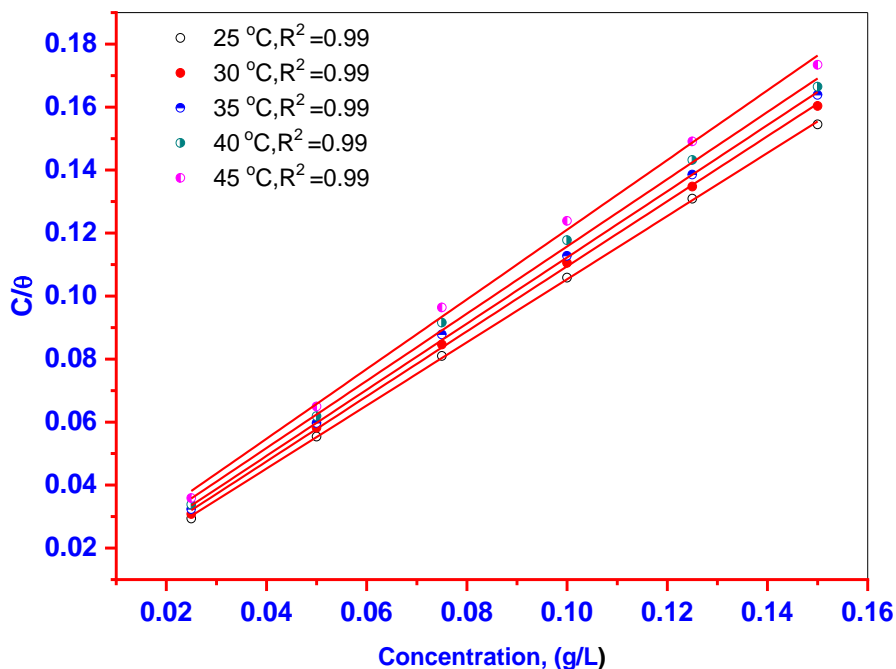| Temp, °C	K_{ads}, M^{-1}	- ΔG^{o}_{ads}, kJ mol^{-1}	-ΔH^{o}_{ads}, kJ mol^{-1}	ΔS^{o}_{ads}, J mol^{-1} K^{-1}
25	194.12	23.07		
30	161.03	22.89		
35	137.93	22.82	31.46	28.21
40	110.04	22.60		
45	95.52	22.51		

Figure 5. Langmuir adsorption plots at different temperatures

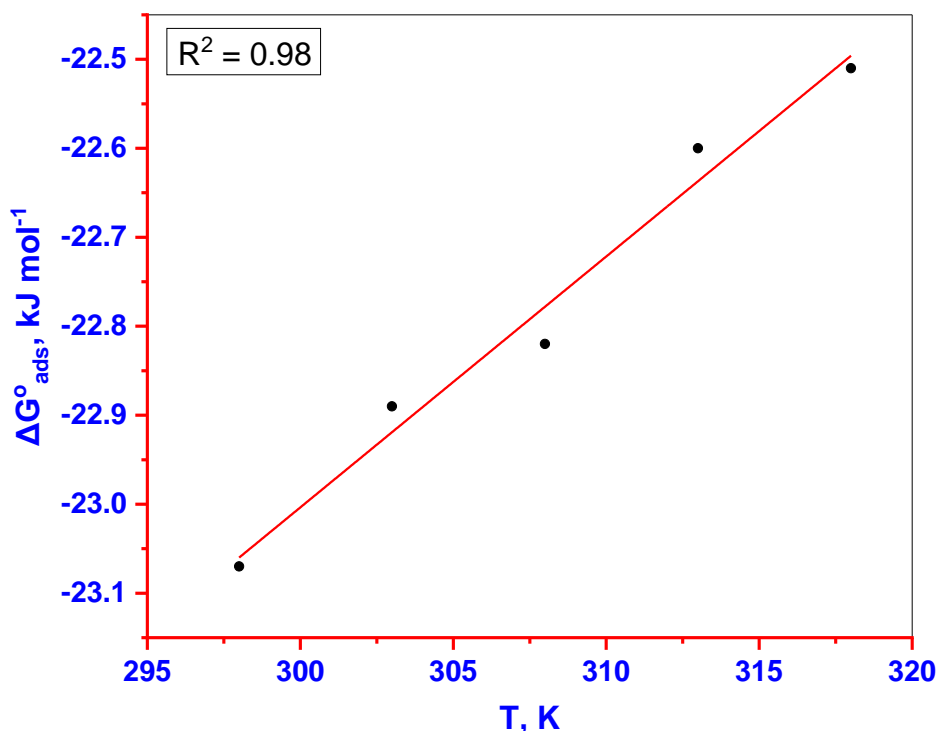*Slika 5. Langmuir-ovi adsorpcioni grafikoni na različitim temperaturama*

Figure 6. ΔG°$_{ads}$ vs. T for α-brass in 1.0 M HNO$_3$ in the presence of CME

Slika 6. ΔG^0$_{ADS}$ u odnosu na T za α-mesing u 1.0 M HNO$_3$ u prisustvu CME

3.4. PDP tests

Figure 7 considers Tafel plots of α-brass solution with and without different concentrations of (CME) extract in 1M HNO$_3$. An estimate of corrosion intensity was obtained by linearly extrapolating branches of the Tafel slopes, and through it, the values of (% IE$_{pp}$) and surface coverage (Ө) were calculated according to the following equation [31].

$$\%IE_{PP} = \left(\frac{i_{corr} - i_{inh}}{i_{corr}}\right) x \ 100 = \ Ө \ x \ 100 \quad (8)$$

As i$_{corr}$ is the corrosion current density without inhibitor and the i$_{(inh)}$ is the corrosion current density

with the extract. We find the corrosion coefficients (E$_{corr}$), corrosion current density (i$_{corr}$), anodic (β$_a$), and cathodic (β$_c$) Tafel constants in Table 4 and Fig. 7, through which we notice a decrease in the values of i$_{corr}$ with the increase in the concentration of the plant extract. We also note the stability of the values of E$_{corr}$ and from the previous results we conclude the mixed behavior of the extract of the CME. The small size of the polarization indicates the equilibrium state of the extract on the surface [30]. In the end, we find that the results of potentiodynamic results agree with the results of weight loss.

Table 4. PDP parameters of α-brass with/ without different concentrations of CME in 1.0 M HNO$_3$ at 25ºC

*Tabela 4. PDP parametri **α** -mesinga sa/bez različitih koncentracija CME u 1.0 M HNO$_3$ na 25ºC*

| Conc., ppm	i$_{corr,}$, µA cm^{-2}	-E$_{corr}$, mV vs SCE	β$_a$, mV dec^{-1}	β$_c$, mV dec^{-1}	θ	% IE$_{PDP}$
Blank	675±0.2215489	2.52±0.098542	0.865±0.009874	-----	-----	-----
25	125±0.1452966	2.61±0.145716	0.793±0.011590	0.551±0.00700	0.815	81.5
50	105±0.1763834	3.69±0.239467	0.603±0.017349	13.7±0.176383	0.844	84.4
75	99.8±0.1201850	1.47±0.086858	0.643±0.014449	23.5±0.230940	0.852	85.2
100	81.2±0.1732050	2.07±0.144491	0.654±0.014437	21.6±0.202758	0.879	87.9
125	27.4±0.1154700	2.68±0.144683	0.613±0.015666	19.2±0.088191	0.959	95.9
150	19.5±0.1527525	2.46±0.117189	0.578±0.008717	18.8±0.033333	0.971	97.1
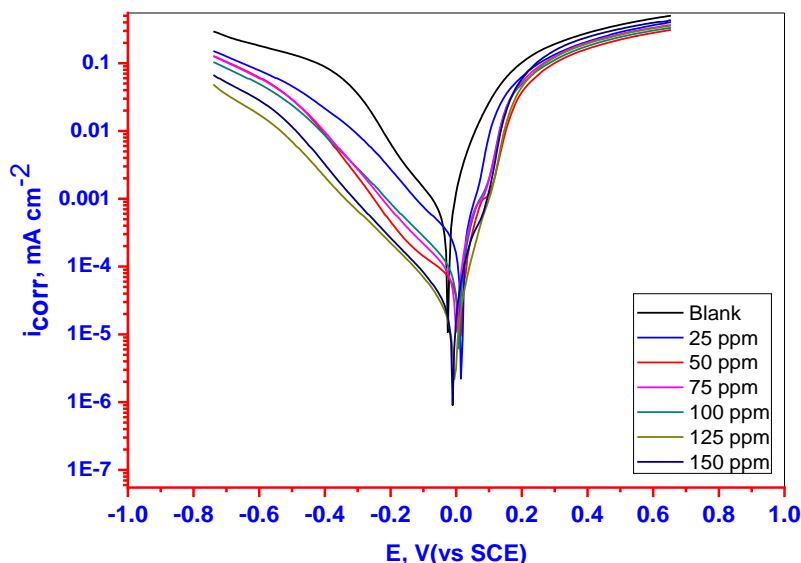
Figure 7. PDP curves of α-brass corrosion in 1.0M HNO₃ solution with/ without different concentrations of CME at 25ºC

Slika 7. PDP krive korozije α -mesinga u 1.0M rastvoru HNO₃ sa/ bez različitih koncentracija CME na 25ºC

3.5. EIS Measurements

Figure 8 displays the Nyquist diagram of alpha brass in 1.0M HNO₃ with various CME concentrations at 25 °C. The graph shows incomplete circles, which confirms that the charge transfer is controlling the α-brass corrosion process. A suitable equivalent circuit (EC) model is obtained by fitting the EIS curves (Figure 8), which include the charge transfer resistance (R_{ct}) in parallel with the capacitance (C_{dl}) connected to the solution resistance (R_s). The values of (R_{ct}), and (C_{dl}) were obtained from fitted EIS plots and listed in Table 5. (% IE$_{EIS}$), and (Θ) were calculated from (R_{ct}) values according to the equation [32]:

$$\%IE_{EIS} = \left| \frac{R_{ct}^{inh} - R_{ct}^{b}}{R_{ct}^{inh}} \right| x\ 100 = \theta\ X\ 100 \quad (9)$$

where R_{ect}^{einj} & R_{ct}^{b} are the value of charge transfer resistance with/ without CME, respectively.

It is clear that from Table 5, with the increase in the concentration of the CME, the values of (R_{ct}) increase and the values of (C_{dl}) decrease, and (% IE$_{EIS}$) increase because of the adsorption that is installed on the surface of the working electrode, which leads to the formation of a layer on the metal [33].

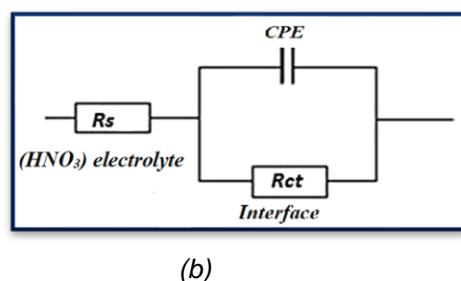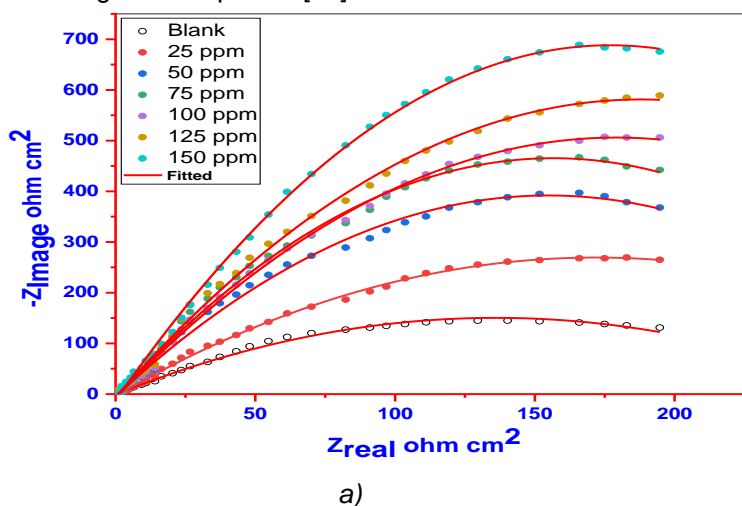|	
a)	*(b)*

Figure 8. Nyquist plots (a), and equivalent circuit (EC) model (b) for α-brass in 1.0 M HNO₃ without/with different concentrations of CME at 25ºC

Slika 8. Nyquist- ovi dijagrami (a) i model ekvivalentnog kola (EC) (b) za α-mesing u 1.0 M HNO₃ bez/sa različitim koncentracijama CME na 25⁰C

Table 5. EIS data of α-brass in 1.0 M HNO₃ in the absence and presence of different concentrations of CME at 25ºC

*Tabela 5. EIS podaci **α** -mesinga u 1.0M HNO₃ u odsustvu i prisustvu različitih koncentracija CME na 25ºC*

Conc., ppm	R_{ct}, Ω cm²	C_{dl}, µF cm⁻²	Ө	% IE_{EIS}
Blank	66.5±0.173228295	259.8±0.1409480	--	--
25	792.60±0.1201850	198.4±0.1732050	0.916	91.6
50	1134.0±0.2027587	114.6±0.2027587	0.941	94.1
75	1520.0±0.1452966	106.7±0.0881917	0.950	95.0
100	1362.0±0.2603416	124.4±0.1855921	0.951	95.1
125	1675.0±0.0881917	152.2±0.1452966	0.956	95.6
150	1326.0±0.1201850	124.7±0.1201850	0.960	96.0

3.6. Scan Electron Microscope (SEM)

The α-brass specimens after 6 hours of immersion at 25ºC in 1.0M HNO₃ solution alone and with adding optimum concentration (150 ppm) of CME were investigated using SEM to evaluate the surface with a protective film. The surface of the pure α-brass sample was smooth (Fig. 9a), while the metal surface became more roughness and damaged with many deep cracks after immersion in the corrosive medium (Fig. 9b). This is due to dissolution of metal in the test solution. On the other hand, the surface became smoother with small deep cracks after the addition of (CME) to the test medium (Fig. 9c). This is attributed to the adsorption of CM) components on the metal surface, leading to the formation of a protective film, which reduces the contact between the metal and the corrosive medium, and therefore, delaying the corrosion rate of α-brass [34].
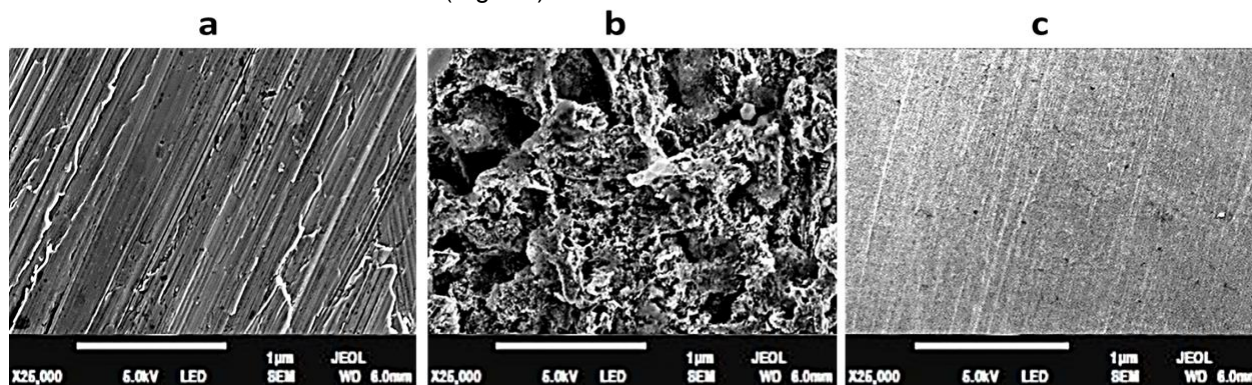

Figure 9. SEM photograph of pure α-brass (a), α-brass with 1.0 M HNO₃, and α-brass with 150 ppm of CME

*Slika 9. SEM fotografija čistog **α**-mesinga (a), **α**-mesinga sa 1.0M HNO₃ i **α**-mesinga sa 150 ppm CME*

3.7. Atomic Force Microscope (Afm)

According to the 3D image of the **α**-mesinga without the studied CME inhibitor, the metal surface has been repeatedly destroyed by the corrosive attacks of the 1M HNO₃ Fig.10b. However, the 3D images (Fig. 10c) showing smoother surfaces than the blank demonstrate that the insertion of an inhibitor reduces corrosion of **α**-mesinga in the aggressive medium. According to the modular software Gwyddion, Table 6 displays the mean roughness (Sₐ) and average RMS roughness (Sq) of the films formed on the Cu surface [35]. According to the data in Table 1, the blank's RMS roughness and mean roughness are higher than those of the inhibitor under study and pure metal, proving the efficiency of the compound in protecting **α**-mesinga's surface from corrosive medium. The AFM results provide additional evidence in favour of the order of inhibitory effectiveness identified by investigations into weight loss and electrochemical tests.

Table 6. AFM parameters of CME compounds

Tabela 6. AFM parametri CME jedinjenja

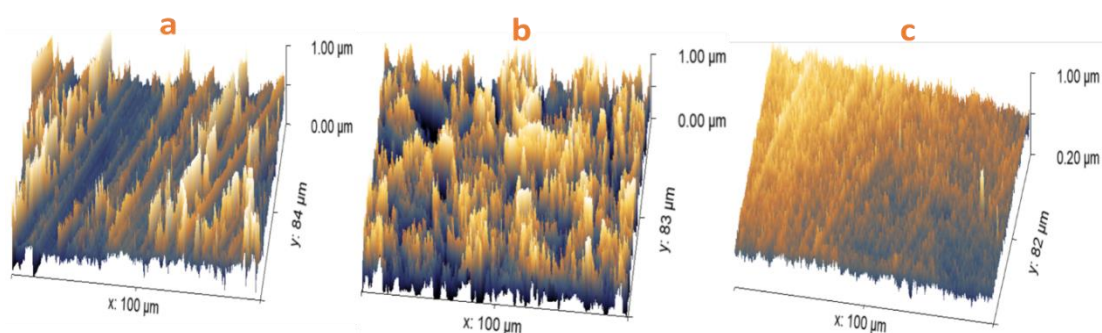| Sample	RMS roughness (Sq), nm	Mean roughness (Sa), nm
a	124.1	83.7
b	237.7	195.5
c	99.6	80.11

Figure 10. AFM photograph of pure α-brass (a), α-brass with 1.0 M HNO₃, and α-brass with 150 ppm of CME

Slika 10. AFM fotografija čistog a-mesinga (a), a-mesinga sa 1.0 M HNO₃ i a-mesinga sa 150 ppm CME

3.8. HOMO-LUMO molecule orbital

An analysis of the impact of stylopine, chelidonine protopine, and Allocryptopine molecule's orientation on inhibition performance was conducted using density function theory (DFT). As shown in Figure 11, the optimized geometry, HOMO surface, and LUMO surface of studied inhibitors can be found in gaseous and aqueous phases. The parameters HOMO (E_H), LUMO (E_L), and dipole moment (μ) for CME gradients were directly obtained from DFT. Equations (10) to (15) were used to calculate the energy gap (ΔE), ionization energy (I), and affinity of electron (A) from which we can calculate the electronegativity (χ), global hardness (η) and softness (σ), and the fraction of transferred electron (ΔN) [36, 37].

$$\Delta E_{L-H} = E_{LUMO} - E_{HOMO} \tag{10}$$

$$\Delta N = \frac{(\phi_{Cu} - \chi_{inh})}{2(\eta_{Cu} + \eta_{inh})} \tag{11}$$

$$\chi_{inh} = \frac{I+A}{2} \tag{12}$$

$$\eta_{inh} = \frac{I-A}{2} \tag{13}$$

$$I = -E_{HOMO} \tag{14}$$

$$A = -E_{LUMO} \tag{15}$$

As χ_{inh} is the electronegativity, which points the capacity of a molecule to attract electrons, η_{inh} is the global hardness, φ is the work function of the Cu surface (4.65 eV) [34], and the (η_{Cu}) for copper = 0 eV, when *I = P*. The $\Box_{inh}$ and η_{inh} are connected with electron affinity (A) and ionization potential (I) of molecules. Numerous articles have discussed how higher values of E_H and lower values of E_L determine the greater electron-donating and accepting abilities of an inhibitor [38]. Inhibitors are more reactive when a lesser value of ΔE is present [39]. In this instance, the protopine molecule's E-value is 1.987 in the gaseous phase while the values for the stylopine, chelidonine protopine, and allocryptopine molecules are, respectively, 2.191, 2.067, and 2.022 in the gaseous phase. In comparison to stylopine, chelidonine, and allocryptopine molecules, these values suggest that the protopine molecule has a high degree of reactivity. Metals and inhibitors can be understood using the number/fraction of electron transfer (ΔN). If the N value of an inhibitor is less than 3.6, it is found to have a stronger capability of donating electrons to metallic surfaces [40]. Compared to stylopine, chelidonine, and allocryptopine molecules, protopine exhibits greater amounts of ΔN in the gaseous phase, indicating that protopine exhibits a stronger inhibitory effect.

Table 7. Quantum chemical parameters of investigated components of CME

Tabela 7. Kvantno hemijski parametri ispitivanih komponenti CME

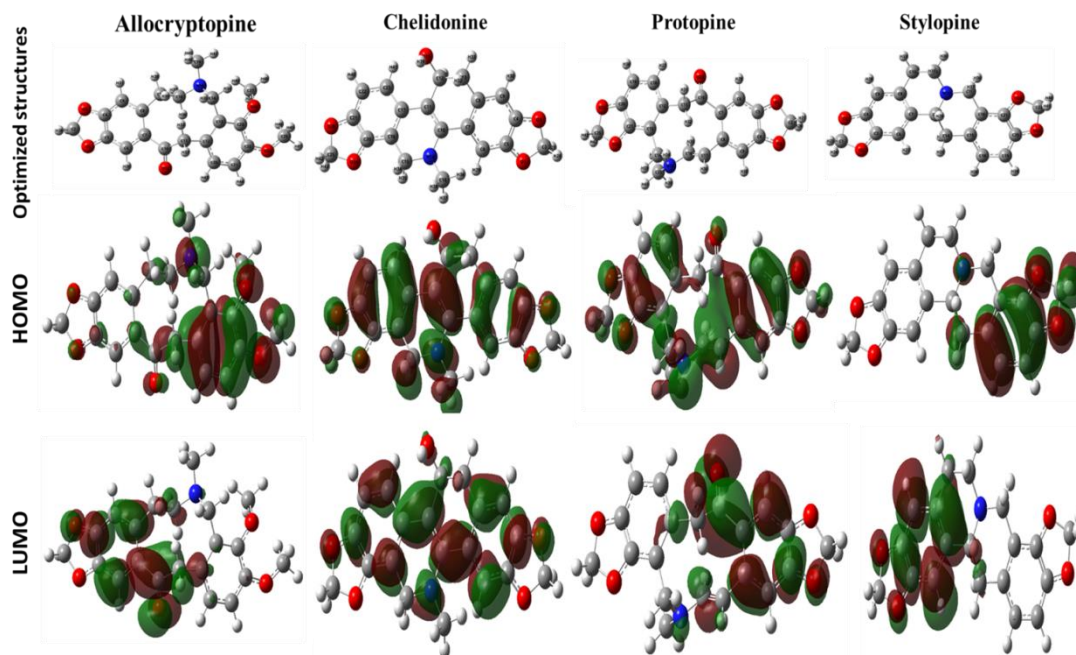| Compound	E_{HOMO}, eV	E_{LUMO}, eV	ΔE, eV	I, eV	A, eV	χ_{inh}, eV/mol	η_{inh}, eV/mol	ΔN
stylopine	-2.314	-0.123	2.191	2.314	0.123	1.218	1.095	0.74
chelidonine	-2.191	-0.167	2.067	2.191	0.167	1.179	1.012	0.79
protopine	-2.136	-0.149	1.987	2.136	0.149	1.142	0.993	0.82
allocryptopine	-2.165	-0. 143	2.022	2.165	0. 143	1.154	1.011	0.80

Figure 11. The optimized geometrical structure (HOMO) and (LUMO) of the four compounds of CME

Slika 11. Optimizovana geometrijska struktura (HOMO) i (LUMO) četiri jedinjenja CME

3.9. Fukui function

One of the important studies that helps us understand how adsorption is on the surface of metals is the study of the Fukui function, through which we can determine which atoms attack the metals as an electrophile or a nucleophile[41]. The Fukui indices are calculated as follow[42]:

$$f_k^+ = [q_k(N+1) - q_k(N)] \quad \textit{Nucleophilic attack}$$

$$f_k^- = [q_k(N) - q_k(N-1)] \quad \textit{Electrophilic attack}$$

$$\Delta f_k(r) = f_k^+ - f_k^- \quad \textit{Dual descriptor}$$

Where, f_k^+ is a nucleophilic attack, f_k^- is an electrophilic attack and $\Delta f_k(r)$ is the dual descriptor.

Figure 12 explain the Mullikan charge distribution for these compounds that can be calculated. Atoms that have $\Delta f_k > 0$ are electrophiles, whereas those that have $\Delta f_k < 0$ are nucleophiles [43].
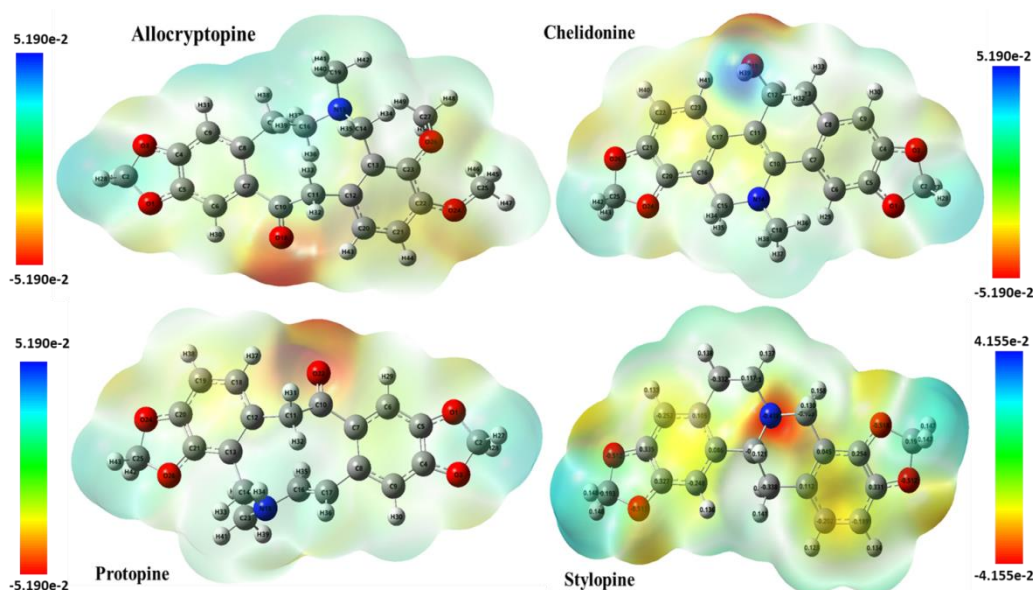

Figure 12. Electrostatic potential maps of CME compounds

Slika 12. Mape elektrostatičkog potencijala CME jedinjenja

It is evident from Table 8 that the Oxygen 18 atom of Stylopine is the preferred nucleophilic site, as it has the highest value of f_k^+ (0.153) and the highest positive value of Δf_k (0.129). In the N15 atom, f_k^- is calculated to be 0.155 and it is negative Δf_k (-0.15), indicating that electrophiles attack this site most frequently. Similar result is obtained in

compounds Protopine, Chelidonine and Allocryptopine in Tables 9-11 with the maximum values of f_k^+ (0.143, 0.079 and 0.103) and Δfk values of (0.093, 0.027, and 0.075) at O22, C10, and C9 atoms and maximum values of f_k^- (0.083, 0.076 and 0.046) and Δf_k values of (− 0.065, − 0.02 and − 0.019) at N15, C11 and O5 atom.

Table 8. Selected calculated Fukui functions and Mulliken atomic charges of Stylopine

Tabela 8. Odabrane izračunate Fukui funkcije i Mullikenove atomske naboje Stilopina

Symbol	f_k^+	f_k^-	Δf_k	Symbol	f_k^+	f_k^-	Δf_k
O (1)	0.023	0.029	-0.006	N (15)	0.005	0.155	-0.15
C (2)	-0.002	-0.001	-0.001	C (16)	-0.007	-0.021	0.014
O (3)	0.041	0.017	0.024	C (17)	-0.017	-0.006	-0.011
C (4)	0.077	0.015	0.062	O (18)	0.153	0.026	0.127
C (5)	0.024	0.026	-0.002	C (19)	-0.005	-0.024	0.019
C (6)	0.066	0.021	0.045	C (20)	0.005	0.012	-0.007
C (7)	0.013	0.022	-0.009	C (21)	0.012	0.014	-0.002
C (8)	0.056	0.005	0.051	C (22)	0.013	0.013	0
C (9)	0.035	0.020	0.015	C (23)	0.009	0.007	0.002
C (10)	0.139	0.010	0.129	O (24)	0.005	0.007	-0.002
C (11)	-0.014	-0.008	-0.006	C (25)	-0.003	-0.003	0
C (12)	-0.013	0.004	-0.017	O (26)	0.003	0.004	-0.001
C (13)	0.012	-0.015	0.027	C (27)	-0.003	-0.005	0.002
C (14)	-0.009	-0.033	0.024	H (25)	0.018	0.028	-0.01

Table 9. Selected calculated Fukui functions and Mulliken atomic charges of Protopine

Tabela 9. Odabrane izračunate Fukui funkcije i Maliken atomski naboji Protopina

Symbol	f_k^+	f_k^-	Δf_k	Symbol	f_k^+	f_k^-	Δf_k
O (1)	0.022	0.039	-0.017	N (15)	0.018	0.083	-0.065
C (2)	-0.002	-0.002	0	C (16)	0.006	0.023	-0.017
O (3)	0.033	0.020	0.013	C (17)	0.023	0.073	-0.05
C (4)	0.062	0.020	0.042	C (18)	0.009	0.017	-0.008
C (5)	0.027	0.039	-0.012	C (19)	0.012	0.019	-0.007
C (6)	0.059	0.036	0.023	C (20)	0.011	0.018	-0.007
C (7)	0.016	0.031	-0.015	C (21)	0.011	0.020	-0.009
C (8)	0.044	0.004	0.04	O (22)	0.143	0.050	0.093
C (9)	0.042	0.034	0.008	C (23)	-0.008	-0.016	0.008
C (10)	0.100	0.001	0.099	O (24)	0.007	0.022	-0.015
C (11)	-0.017	-0.015	-0.002	C (25)	-0.000	-0.001	0.001
C (12)	-0.009	0.009	-0.018	O (26)	0.005	0.019	-0.014
C (13)	0.005	-0.002	0.007	H (27)	0.018	0.018	0
C (14)	-0.009	-0.014	0.005	H (28)	0.019	0.019	0

Table 10. Parameters of Fukui functions and Milliken atomic charges were calculated of Chelidonine

Tabela 10. Parametri Fukui funkcija i Milikenov atomski naboj su izračunati za Shelidonin

Symbol	f_k^+	f_k^-	Δf_k	Symbol	f_k^+	f_k^-	Δf_k
O (1)	0.016	0.018	-0.002	C (15)	-0.007	-0.013	0.006
C (2)	-0.002	-0.002	0	C (16)	0.034	0.025	0.009
O (3)	0.027	0.027	0	C (17)	0.020	0.016	0.004
C (4)	0.058	0.030	0.028	C (18)	-0.010	-0.012	0.002
C (5)	0.020	0.019	0.001	O (19)	0.014	0.015	-0.001
C (6)	0.045	0.018	0.027	C (20)	0.019	0.025	-0.006
C (7)	0.025	0.008	0.017	C (21)	0.050	0.046	0.004
C (8)	0.031	0.022	0.009	C (22)	0.024	0.029	-0.005
C (9)	0.030	0.020	0.01	C (23)	0.036	0.047	-0.011
C (10)	0.079	0.052	0.027	O (24)	0.013	0.020	-0.007
C (11)	0.056	0.076	-0.02	C (25)	-0.001	-0.002	0.001
C (12)	-0.007	-0.011	0.004	O (26)	0.023	0.039	-0.016
C (13)	-0.008	-0.009	0.001	H (27)	0.015	0.015	0
N (14)	0.016	0.048	-0.032	H (28)	0.014	0.014	0

Table 11. Parameters of Fukui functions and Mullikan atomic charges were calculated of Allocryptopine

Tabela 11. Parametri Fukui funkcija i Mullikanov atomski naboj su izračunati za Alokriptopin

Symbol	f_k^+	f_k^-	Δf_k	Symbol	f_k^+	f_k^-	Δf_k
C (1)	-0.003	-0.003	0	C (15)	0.015	0.025	-0.01
O (2)	0.026	0.044	-0.018	C (16)	0.040	0.018	0.022
C (3)	0.039	0.030	0.009	C (17) -	-0.008	-0.009	0.001
C (4)	0.046	0.031	0.015	C (18)	0.035	0.038	-0.003
O (5)	0.027	0.046	-0.019	C (19)	0.052	0.027	0.025
C (6)	0.103	0.025	0.078	C (20)	0.022	0.034	-0.012
C (7)	0.028	0.025	0.003	C (21)	0.036	0.035	0.001
C (8)	0.021	0.028	-0.007	O (22)	0.015	0.051	-0.036
C (9)	0.103	0.028	0.075	C (23) -	-0.001	-0.003	0.002
C (10)	-0.011	-0.016	0.005	O (24)	0.015	0.046	-0.031
N (11)	0.002	0.042	-0.04	H (28)	0.022	0.016	0.006
C (12)	-0.008	-0.012	0.004	H (29)	0.019	0.014	0.005
C (13)	-0.005	-0.006	0.001	H (30)	0.048	0.019	0.029
C (14)	-0.008	-0.007	-0.001	H (30)	0.048	0.018	0.03

3.10. Monte Carlo Simulation

An assessment of the adsorption of possible interactions between each inhibitor molecule and the Cu(110) surface was conducted using Monte Carlo simulations (MC) [44]. Choosing the Cu(110) plane was based on its good stability and well-packed structure. Forcite module was used to optimize the geometry of CME compounds. A ten-by-ten supercell with a vacuum thickness of thirty microns was modeled with respect to Cu (110) surface. Simulation annealing was used to calculate fine-quality adsorption using five cycles of 50,000 steps. This study investigates low-energy configurations of Cu(110)-inhibitor system in aqueous solution. In order to simulate corrosion in a real-life scenario, the simulation was conducted in an aqueous environment with water molecules. With the COMPASS force field and adsorption locator module, we studied adsorption of the four inhibitors on Cu(110) [45]. Materials Studio 2017 was used to conduct the MC simulation. Table 12 presents the total energy of Cu-inhibitor (E_{Tot}), the adsorption energy (E_{Ads}), rigid adsorption energy (E_{Rigid}), and the deformation energy (E_{Def}) resulting from relaxation of the inhibitor molecule on Cu(110). System stability is correlated with the total energy (E_{Tot}) of the substrate-adsorbate system. The negative E_{tot} indicates the stabilization of all the particles (Cu, and H_2O) in the simulation box. Furthermore, corrosion inhibitors adsorb strongly to

metal surfaces, causing low E_{Ads} [46]. All the compounds display low adsorption energy. The adsorption energy of all compounds are negative values which suggests a spontaneously relaxed configuration of the adsorbate-substrate system [47]. Here are four views of molecules adsorbed on the surface of Cu(110) in aqueous solution, as shown in figure 13. Parallel arrangement of inhibitors on the Cu surface suggests that they can adsorb well through covalent and non-covalent interactions with the metal surface [48], and to back-donate to low-lying d-orbitals of Cu (110), insulating the Cu from the corrosion environment.

Table 12. Monte Carlo simulation parameters of adsorption of CME compounds on Cu (1 1 0) surface

Tabela 12. Monte Karlo simulacioni parametri adsorpcije CME jedinjenja na površini Cu (1 1 0)

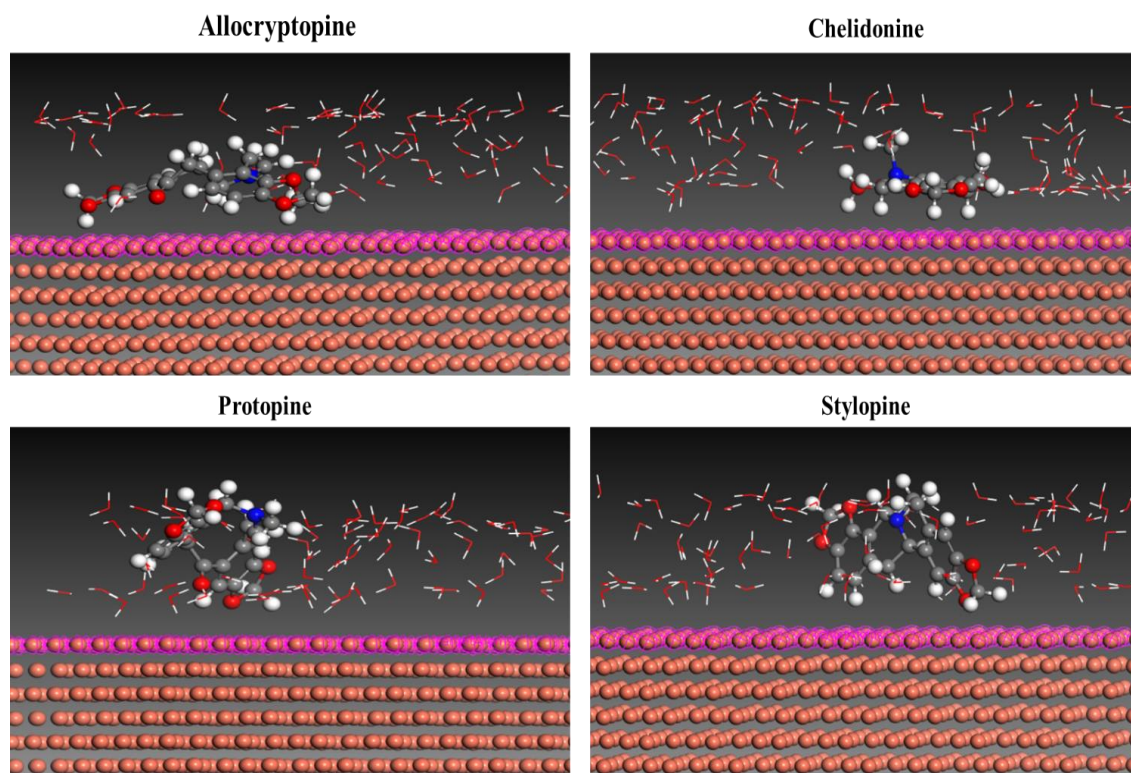| Structure	E_{Tot}	E_{Rigid}	E_{Def}	$E_{Ads} = E_{Rigid} + E_{Def}$
Cu (1 1 0) − stylopine	-1240.538	-1303.199	58.808	-1244.391
Cu (1 1 0) − chelidonine	-1241.488	-1327.332	56.251	-1271.080
Cu (1 1 0) − protopine	-1210.537	-1297.337	60.163	-1237.173
Cu (1 1 0) − Allocryptopine	-1219.387	-1309.631	-319.946	-1629.578

Figure 13. Adsorption of CME compounds on Cu surface in aqueous medium

Slika 13. Adsorpcija CME jedinjenja na površini Cu u vodenoj sredini

3.11 Mechanism of corrosion inhibition

The inhibitive action behavior of some plant extracts is attributed to the adsorption of the phyto-chemical constituents that exist in the leaves extract on the metal surface, which protects the metal surface and thus does not permit the corrosion process to take place. The adsorption of the inhibitor depends on the chemical structure of the phyto-components in the inhibitor, the charge on the metal surface, and the nature of the corrosive medium. In our study, the Cu surface in an acidic medium carry a positive charge, therefore, the electrostatic repulsion takes place between the inhibitor molecules and the metal surface. Nitrate ions (NO_3^-) get adsorbed on the metal surface creating an extra negative charge near the corrosive solution and approving more adsorption for the inhibitor molecules to adsorb on the Cu surface due to the electrostatic interaction (physical adsorption) [49]. On the other hand, the chemisorption processes are created via the donation of electrons lone pairs on heteroatoms

such as N, O, and π -electrons in aromatic rings to get bonded to the vacant d-orbital of Cu ions. Once the surface is saturated with an electron, the surface becomes more negatively charged. Then to release the excess electron from the surface, the electron present in the d-orbital of Cu gets transferred to the vacant π- antibonding orbital of the inhibitor molecules (retro-donation) [50]. Thus forming a stable barrier film effectively inhibits the anodic and cathodic reactions of copper in the HNO_3 medium (see Fig .14). From all of this, we conclude that the high % IE is due to a group of basic factors that lead to the adsorption of compounds on the surface of the metal. The %IE of CME in the current study is compared with previously reported in the literature in acidic media and recorded in Table 13. It is clear that the CME gave 96 % IE at 150 ppm, so it acts as a good corrosion inhibitor for α-brass in a nitric acid environment.
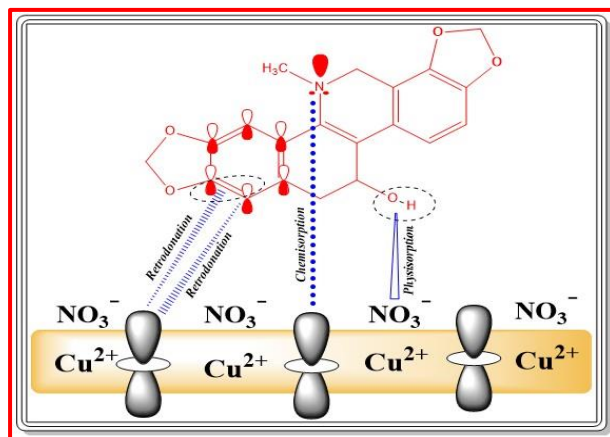

Figure 14. The schematic representation of (CME) on the α- brass surface in 1.0 M HNO_3 medium

Slika 14. Šematski prikaz (CME) na površini α-mesinga u medijumu 1.0 M HNO_3

Table 13. A comparison of CME with some other studied (%IE is reported at the maximum) extracts

Tabela 13. Poređenje CME sa nekim drugim proučavanim (%IE je prijavljen kao maksimum) ekstraktima

Source of extract	Test medium	Metal/Alloy	% IE	References
Orange peels	HCl and H_2SO_4	Cu	43.0	[38]
Mangrove tannin	HCl	Cu	82.4	[39]
Myrtus communis	H_2SO_4	Cu	>85.0	[40]
Alhagi maurorum plant extract	H_2SO_4	Cu	33.0-83.0	[41]
Egyptian licorice extract	HCl	Cu	55.0-89.0.0	[42]
Exudate gum from *Dacryodes edulis*	HCl	Al	42.0	[43]
Opuntia ficus indica	HCl	C-steel	70.0-91.0	[44]
Chelidonium Majus (Papaveraceae)	HNO_3	α-brass	96	Our results

4. CONCLUSION

The current study demonstrated the possibility of using Papaveraceae extract in inhibiting α-brass in nitric acid corrosion. The inhibition process comes is due to not only the surface adsorption but also a synergistic effect. It was found that the inhibitory process is controlled by temperature and inhibitor concentration. SEM investigation for α-brass surface revealed the presence of a protective film, which protect α-brass alloy against the corrosive media. DFT calculations pointed out that the CME mainly interact with α-brass surface via the donor-acceptor mechanism.

5. REFERENCES

[1]   L.K.Goni et al. (2022) Acridine and Its Derivatives: Synthesis, Biological, and Anticorrosion Properties. Materials, 15(21), 7560.

[2]   A.Zakeri, E.Bahmani, A.S.R.Aghdam (2022) Plant extracts as sustainable and green corrosion inhibitors for protection of ferrous metals in corrosive media: A mini review. Corrosion Communications, 5, 25-38.

[3]   A.M.Abdel-Karim, A.M.El-Shamy (2022) A review on green corrosion inhibitors for protection of archeological metal artifacts. Journal of Bio-and Tribo-Corrosion, 8(2), 35-42.

[4]   B.Vaghefinazari et al. (2022) Chromate-Free Corrosion Protection Strategies for Magnesium Alloys—A Review: Part III—Corrosion Inhibitors and Combining Them with Other Protection Strategies. Materials,15(23), 8489.

[5]   R.Samiee et al. (2019) Assessment of the smart self-healing corrosion protection properties of a water-base hybrid organo-silane film combined with non-toxic organic/inorganic environmentally friendly corrosion inhibitors on mild steel. Journal of cleaner production, 220, 340-356.

[6]   L.Kong et al. (2022) Application potential of alkali-activated concrete for antimicrobial induced corrosion: A review. Construction and Building Materials,. 317, 126169.

[7]   C.M'Bouillé et al. (2022) Theoretical Evaluation of Some Compounds with Antifungal Effect as Corrosion Inhibitors for Copper in Nitric Acid Solution: DFT Calculations. International Research Journal of Pure and Applied Chemistry, 23(1), 30-42.

[8]   L.V.Hublikar et al. (2021) Biogenesis of Silver Nanoparticles and Its Multifunctional Anti-Corrosion and Anticancer Studies. Coatings, 11(10), 1215.

[9]   Z.Lin, X.Sun, H.Yang (2021) The role of antibacterial metallic elements in simultaneously improving the corrosion resistance and antibacterial activity of magnesium alloys. Materials & Design, 198, 109350.

[10] A.Fouda et al. (2019) CalicotomeExtract as a friendly corrosion inhibitor forCarbon steel in polluted NaClSolution: chemical and electrochemical studies. Egyptian Journal of Chemistry, 62(10),1879-1894.

[11] N.Kumar, M.Mani (2022) Pharmacognostical Evaluation And Quantitative Estimation Of Hibiscus Rosa Sinensis. Journal of Positive School Psychology, 2022, 2236-2248.

[12] S.Joycee et al. (2022) Corrosion mitigation by an eco-friendly inhibitor: Beta vulgaris (beetroot) extract on mild steel in simulated oil well water medium. Int. J. Corros. Scale Inhib, 11(1), 82-101.

[13] S.Devikala et al. (2019) Green Corrosion inhibition of mild steel by Asafoetida extract extract in 3.5% NaCl. Materials Today: Proceedings,14, 590-601.

[14] S.H.M.Jessima, S.Subhashini, J.Arulraj (2020) Sunova spirulina powder as an effective environmentally friendly corrosion inhibitor for mild steel in acid medium. Journal of Bio-and Tribo-Corrosion,6, 1-13.

[15] L.T.Popoola (2019) Progress on pharmaceutical drugs, plant extracts and ionic liquids as corrosion inhibitors. Heliyon, 5(2), e01143.

[16] J.Panchal et al. (2021) Comprehensive review and critical data analysis on corrosion and emphasizing on green eco-friendly corrosion inhibitors for oil and gas industries. Journal of Bio-and Tribo-Corrosion,7(3), 107.

[17] M.Ramezanzadeh, G.Bahlakeh, B.Ramezanzadeh (2020) Probing molecular adsorption/interactions and anti-corrosion performance of poppy extract in acidic environments. Journal of Molecular Liquids, 304,112750.

[18] A.Berrissoul, et al. (2022) Assessment of corrosion inhibition performance of origanum compactum extract for mild steel in 1 M HCl: Weight loss, electrochemical, SEM/EDX, XPS, DFT and molecular dynamic simulation. Industrial Crops and Products, 187, 115310.

[19] M.Sabour, G.Dezvareh, R.Bazzazzadeh (2019) Corrosion prediction using the weight loss model in the sewer pipes made from sulfur and cement concretes and Response Surface Methodology (RSM). Construction and Building Materials, 199,40-49.

[20] N.B.Iroha, L.A.Nnanna (2020) Leucas Martinicensis as an inhibitor of carbon steel corrosion in acidic medium. Int J Res, 7, 19-26.

[21] N.Benzbiria, M.Zertoubi, M.Azzi (2021) Influence of copper surface pretreatment on the kinetics of oxygen reduction reaction in 0.5 M NaCl solution: Surface characterization and electrochemical studies. Applied Surface Science Advances, 4, 100069.

[22] R.A.Costa et al. (2021) Experimental and theoretical study on spectral features, reactivity, solvation, topoisomerase I inhibition and in vitro cytotoxicity in human HepG2 cells of guadiscine and guadiscidine aporphine alkaloids. Journal of Molecular Structure,1229,129844.

[23] G.Cui et al. (2019) Chitosan oligosaccharide derivatives as green corrosion inhibitors for P110 steel in a carbon-dioxide-saturated chloride solution. Carbohydrate polymers, 203, 386-395.

[24] O.A.Akinbulumo, O.J.Odejobi, E.L.Odekanle (2020) Thermodynamics and adsorption study of the corrosion inhibition of mild steel by Euphorbia heterophylla L. extract in 1.5 M HCl. Results in Materials, 5, 100074.

[25] O.Sanni, A.Popoola, O.Fayomi (2019) Temperature effect, activation energies and adsorption studies of waste material as stainless steel corrosion inhibitor in sulphuric acid 0.5 M. Journal of Bio-and Tribo-Corrosion, 5, 1-8.

[26] A.S.Fouda et al.(2020) Synthesis, characterization, and application of new nonionic surfactant as a corrosion inhibitor for carbon steel in 1 M hydrochloric acid solution. Journal of Bio-and Tribo-Corrosion, 6, 1-9.

[27] A.S.Fouda, A.Wahba, M.Eissa (2022) Aluminum corrosion prevention in 1.0 M HCl solution by cystosiera myrica extract: An experimental and biological study. Journal of the Indian Chemical Society, 99(8), 100619.

[28] A.M.Al-bonayan, A.M.Wahba, A.S.Fouda (2022) Corrosion Prevention of Al in 1.0 M Hydrochloric Acid Using Novel Plant Extract: Chemical, Electrochemical, and Surface Analysis Studies. Protection of Metals and Physical Chemistry of Surfaces, 58(4), 834-844.

[29] A.Pal, C.Das (2022) Investigations on corrosion inhibition in acidic media for BQ steel using banana flower bract, an eco-friendly novel agro-waste: Experimental and theoretical considerations. Inorganic Chemistry Communications, 145, 110024.

[30] A.S.Fouda, S.Etaiw, A.Wahba (2015) Effect of acetazolamide drug as corrosion inhibitor for carbon steel in hydrochloric acid solution., Nat Sci, 13(9), 1-8.

[31] S.Esmailzadeh, M.Aliofkhazraei, H.Sarlak (2018) Interpretation of cyclic potentiodynamic polarization test results for study of corrosion behavior of metals: a review. Protection of metals and physical chemistry of surfaces, 54, 976-989.

[32] Jr,S.Feliu (2020) Electrochemical impedance spectroscopy for the measurement of the corrosion rate of magnesium alloys: Brief review and challenges. Metals, 10(6), 775.

[33] N.Iroha, L.Nnanna (2019) Electrochemical and Adsorption Study of the anticorrosion behavior of Cefepime on Pipeline steel surface in acidic Solution. J. Mater. Environ. Sci, 10(10), 898-908.

[34] A.Thakur, A.Kumar (2021) Sustainable inhibitors for corrosion mitigation in aggressive corrosive media: a comprehensive study. Journal of Bio-and Tribo-Corrosion, 7, 1-48.

[35] M.Proença et al. (2022) Optimization of Au: CuO thin films by plasma surface modification for high-resolution LSPR gas sensing at room temperature. Sensors, 22(18), 7043.

[36] N.Obi-Egbedi, I.Obot, M.I.El-Khaiary (2011) Quantum chemical investigation and statistical analysis of the relationship between corrosion inhibition efficiency and molecular structure of

xanthene and its derivatives on mild steel in sulphuric acid. Journal of Molecular Structure, 1002(1-3), 86-96.

[37] I.Obot, N.Obi-Egbedi (2010) Theoretical study of benzimidazole and its derivatives and their potential activity as corrosion inhibitors. Corrosion Science, 52(2), 657-660.

[38] N.Mazlan et al. (2022) Density functional theory and molecular dynamics simulation studies of bio-based fatty hydrazide-corrosion inhibitors on Fe (1 1 0) in acidic media. Journal of Molecular Liquids, 347, 118321.

[39] A.Singh et al. (2020) Comprehensive investigation of steel corrosion inhibition at macro/micro level by ecofriendly green corrosion inhibitor in 15% HCl medium. Journal of colloid and interface science,560, 225-236.

[40] R.Hsissou et al. (2021) Insight into the corrosion inhibition of novel macromolecular epoxy resin as highly efficient inhibitor for carbon steel in acidic mediums: Synthesis, characterization, electroche-mical techniques, AFM/UV–Visible and computa-tional investigations. Journal of Molecular Liquids, 337, 116492.

[41] H.M.Qadr, D.M.Mamand (2021) Molecular structure and density functional theory investigation corrosion inhibitors of some oxadiazoles. Journal of Bio-and Tribo-Corrosion,7(4), 140.

[42] N.Ammouchi et al. (2020) DFT computations and molecular dynamics investigations on conformers of some pyrazinamide derivatives as corrosion inhibitors for aluminum. Journal of molecular liquids, 300,112309.

[43] O.A.Odewole et al. (2021) Synthesis and anti-corrosive potential of Schiff bases derived 4-nitrocinnamaldehyde for mild steel in HCl medium:

[44] D.K.Verma et al. (2021) Investigations on some coumarin based corrosion inhibitors for mild steel in aqueous acidic medium: Electrochemical, surface morphological, density functional theory and Monte Carlo simulation approach. Journal of Molecular Liquids, 329, 115531.

[45] O.E.Oyeneyin (2022) Investigation of Corrosion Inhibition Potential of Triazolopyrimidinones via Density Functional Theory and Monte-Carlo Simulations. Science Letters, 10(3), 95-105.

[46] E. Berdimurodov et al. (2022) Novel gossypol–indole modification as a green corrosion inhibitor for low–carbon steel in aggressive alkaline–saline solution. Colloids and Surfaces A: Physicochemical and Engineering Aspects, 637, 128207.

[47] F.El-Hajjaji et al. (2019) 1-Octyl-2-(octylthio)-1H-benzimidazole as a new and effective corrosion inhibitor for carbon steel in 1 M HCl. Portugaliae Electrochimica Acta, 37(3), 131-145.

[48] S.Satpati et al. (2023) Interaction of newly synthesized dipeptide Schiff bases with mild steel surface in aqueous HCl: Experimental and theoretical study on thermodynamics, adsorption and anti-corrosion characteristics. Materials Chemistry and Physics, 296, 127200.

[49] I.W.Ma et al. (2022) A concise review on corrosion inhibitors: types, mechanisms and electrochemical evaluation studies. Journal of Coatings Technology and Research, 19, 1-28.

[50] C.Verma et al. (2018) Sulfur and phosphorus heteroatom-containing compounds as corrosion inhibitors: An overview. Heteroatom Chemistry,. 29(4), e21437.

IZVOD

EKSPERIMENTALNA I TEORIJSKA OPTIMIZACIJA EKSTRAKTA *Chelidonium Majus (Papaveraceae)* KAO EKOLOŠKI PRIHVATLJIVOG INHIBITORA KOROZIJE α -MESINGA U RASTVORU AZOTNE KISELINE

U radu se razmatra proučavanje nivoa inhibicije biljnog ekstrakta Chelidonium Majus (Papaveraceae) (CME) na α-mesingu u 1,0M rastvoru HNO₃. Studija je sprovedena primenom hemijskih i elektrohemijskih tehnika, koje su pokazale rezultate do 97% inhibicije sa 150 ppm na 250⁰C. Za rezultate polarizacije, CME je inhibitor mešovitog tipa. Povećanje otpora prenosa naelektrisanja i smanjenje kapacitivnosti dvostrukog sloja sa povećanjem koncentracije primećeno je Nyquist-ovim dijagramima i utvrđeno je da proces inhibicije prati Langmirovu izotermu koja dokazuje formiranje monosloja na površini α-mesing. Kvantno hemijski proračuni su izvršeni DFT metodom za određivanje aktivnih centara CME koji su odgovorni za adsorpciju, kao i za njihov mogući mehanizam interakcije sa mesinganom površinom.

Ključne reči: *Inhibicija korozije, α- mesing, HNO₃, ekstrakt Chelidonium Majus, DFT*